JOURNAL OF AIRCRAFT
Vol. 42, No. 6, November–December 2005

Stall Hysteresis of an Airfoil with Slotted Flap

Kasim Biber*
Istanbul 34870, Turkey

Stall hysteresis discovered in the wind-tunnel performance of a GA(W)-2 airfoil with a 25% chord slotted flap is examined further by using the data obtained for lift, pitching moment, surface pressure distribution, and the hot-film velocity vector. Test cases include 30- and 40-deg flap deflections, each having an optimum and narrow gap at a chord Reynolds number of 2.2×10^6 and a Mach number of 0.13. The flap optimized to produce the highest $C_{l\max}$ for each flap angle apparently did not have a proper contour and nose location for the slot flow to function effectively at off-design conditions. It is shown that suction pressures over the flap, suppressed by a thickening wing wake at stall, are not reversible to their prestall values within the decreasing α side of loop. It is suggested that the flap design include the use of a new flap parameter called the slot flow angle to describe the slot flow orientation and a pressure recovery factor to select a proper contour for the flap upper surface.

Nomenclature

C_l	=	lift coefficient
$C_{l\max}$	=	maximum lift coefficient
C_m	=	pitching moment coefficient
$C_{P\min}$	=	minimum pressure coefficient
$C_{P@0.95c}$	=	pressure coefficient at 95%c upper surface
C_{PR}	=	pressure recovery coefficient factor
C_p	=	static pressure coefficient, $(p - p_\infty)/q_\infty$
c	=	mean chord of flap-nested airfoil
G/c	=	gap-to-chord ratio
O/c	=	flap-overlap-to-chord ratio
p	=	local static pressure
p_∞	=	freestream static pressure
q_∞	=	freestream dynamic pressure
Re	=	chord-based Reynolds number
X_f, Y_f	=	flap pivot coordinates, X_f along airfoil chord line
x, y	=	airfoil coordinates, x along chord line
α	=	angle of attack, deg
β	=	slot flow angle at flap gap location, deg
δ	=	flap deflection angle, deg

I. Introduction

STALL hysteresis as demonstrated in a wind tunnel is a phenomenon where by the stall inception and stall recovery do not occur at the same angle of attack. If present, it can result in severe control problems in stall. The hysteresis has commonly been observed[1–3] for some single airfoils operating at Reynolds numbers below 10^6. At low Reynolds number, there is usually a laminar separation bubble that characterizes the flow over airfoils. The bubble, if short, contracts in size and trips the boundary layer into turbulent flow with increasing α. It bursts at stall, and this causes an abrupt fall in C_l. Angle of attack may have to be reduced significantly for an attached flow on the upper surface. In the process, the lift coefficient is not restored, causing a reduction in $C_{l\max}$. The stall hysteresis is sensitive to changes in wind-tunnel flow quality and acoustics.[2] It decreases in size and eventually disappears with Reynolds number. However, it is reported by Biber and Zumwalt[4] that the hysteresis reappears at a relatively high Re of 2.2×10^6 for the GA(W)-2 airfoil equipped with 25%c slotted flap.

The hysteresis on the flapped airfoil also occurred in the stall region and caused an average 25% drop in lift coefficient. Its size was shown to vary as function of flap angle and gap. Similar results were also recently reported[5] in wind-tunnel tests of a three-element airfoil, but at a relatively low Re of 1×10^6. In these tests, flap deployment is clearly shown to result in stall hysteresis. Figure 1 illustrates the flowfield for a typical flap position. There is a slot flow between the boundary layers from the cove and flap upper surface. For optimum performance, the slot flow extends downstream so that the boundary layers do not merge until a location about the flap trailing edge.[6] The slot flow magnitude is determined by the gap, but its orientation with respect to the main wing varies primarily with overlap setting. The flap parameters are optimized to obtain the best airfoil performance. However, this has traditionally been done by only increasing α. The hysteresis appears to be an off-design phenomenon and occurs only if the airfoil α is lowered from its poststall range. A proper flap setting should provide a desired performance not only at design but also at off-design conditions. This requires a through understanding of the flap flowfield, including the slot flow. Smith[7] gives details of slot flow effects on high-lift airfoils, but his discussion does not consider the hysteresis.

In this paper, the flap flowfield has been examined by using the wind-tunnel data obtained for C_P distribution, velocity vectors, and flow visualization, in addition to the companion paper,[4] which has limited data and concentrates on airfoil force and moment characteristics. Detailed surface pressure distribution data allow the definition of a pressure recovery factor for each airfoil element. Also, an attempt is made to guide flap designers by using the slot flow angle as a new flap parameter. The procedure for wind-tunnel tests and flap optimization is also given for completeness. The paper is based on the overall experimental program[8] conducted for five test cases of a flapped GA(W)-2 airfoil. Flowfield data for the same airfoil are also reported in a separate paper.[9]

II. Experimental Methodology

A. Wind Tunnel and Test Model

The tests were conducted at Wichita State University (WSU) subsonic wind tunnel with a 2.13×3.05 m (7×10 ft) test section fitted with a 2.13-m (7-ft) high and 0.914-m (3-ft) wide two-dimensional insert,[10] which forms a closed-return tunnel with atmospheric test-section static pressure. The tunnel is equipped with a pyramidal-type balance that measures forces and moments with linearized wall corrections, as an average of 10 readings 0.2 s apart. The test model was made of a rectangular wing of a 13%c thick GA(W)-2 airfoil with a 25%c single-slotted flap, having a reference chord of 0.61 m (2 ft) at the flap-nested position and a span of 0.914 m (3 ft). The airfoil has its maximum thickness of 0.13c at 0.38c and a camber of 0.0218c at the 0.628c location. Along the midspan of the main wing and

Presented in part as Paper 1995-0440 at the 33rd Aerospace Sciences Meeting and Exhibit, Reno, NV, 9–12 January 1995; received 1 July 2004; revision received 28 October 2004; accepted for publication 28 October 2004.

*Engineering Consultant, Karliktepe Mah, Serap Sok, No 4/10, Kartal; kxbiber@yahoo.com. Senior Member AIAA.

flap, there were 69 pressure taps connected to pressure transducers for surface pressure measurements. The model was connected to the external balance system and pivoted at the 0.5c station, with the tunnel centerline considered horizontal.

B. Test Conditions

Tests were made at a Reynolds number (based on flap-nested mean chord) of 2.2×10^6, dynamic pressure of 1150 N/m^2 (24 lb/ft^2), and Mach 0.13. The test-section turbulence level was less than 1%. Boundary-layer transition on the main airfoil element was fixed at the 5%c upper and 10%c lower surfaces by using 2.4-mm- (0.1-in.-) wide trip strips. The flow two dimensionality in the test section was evaluated by visualization of separated flow patterns on the model. Tempera and kerosene flow showed a change in two-dimensional flow character near the sidewalls with the airfoil stalled. Beyond the stall, a spanwise surface flow component within the separated zone appeared and extended toward the juncture of the model and sidewall, where a vortex pair formed and shed at the model trailing edge. However, this was limited to the outer 25% of the span. No boundary-layer control was employed to reduce the three-dimensional flow patterns. The sidewall boundary layer did not have a significant effect on the airfoil stall characteristics. This was probably due to the relatively short upstream length of the sidewalls, 1.06 m (3.5 ft) from the model leading edge. In addition to tempera and kerosene, tufts were attached to the model upper surface to supplement the preceding results.

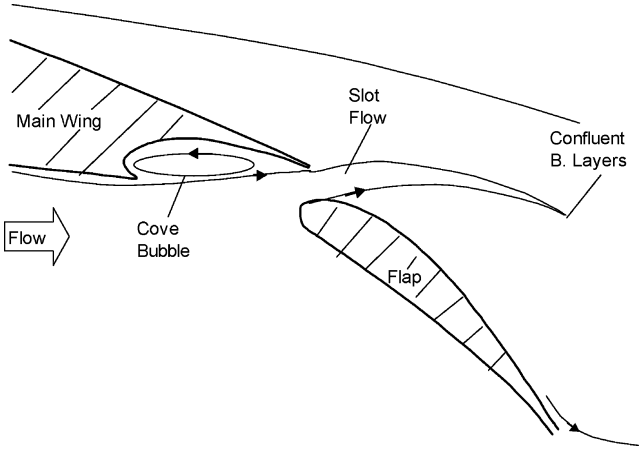

Fig. 1 Slot flow extension over flap.

C. Data Collection and Uncertainty

Lift, drag, and pitching moment were measured for all test configurations using the tunnel external balance and were reduced to coefficient form as C_l, C_d, and C_m. The results for force and moment agree reasonably well with the Ref. 10 data, but the α range of present tests, from -8 to about 20 deg, was relatively higher. The large α range within tunnel safety limits allowed the airfoil to be evaluated for hysteresis for both flap-nested and deflected cases. The model was initially set to $\alpha = 0$ deg at windoff, and then the tunnel speed was increased to that corresponding to the test Re of 2.2×10^6. Once the airflow was stabilized in the tunnel, α was first decreased to -8 deg and then increased to a poststall value following a prescribed schedule having smaller intervals near the stall. After reaching its maximum, α was lowered back to -8 deg with the same schedule as before, without stopping the tunnel to study the hysteresis effects. The data uncertainties are as follows: for lift, ± 0.9 N and ± 0.001 (ΔC_l), for drag ± 0.2 N and ± 0.0003 (ΔC_d), for pitching moment ± 0.1 N $\cdot$ m and ± 0.0003 (ΔC_m), for pressure transducers ± 2.4 N/m^2 and ± 0.004 (ΔC_p), for angle of attack ± 0.05 deg, and for flap angles ± 0.5 deg.

D. Flap Setting and Parameters

Wind-tunnel tests were made in a test matrix of flap settings as shown in Table 1. The test matrix includes flap-nested and -deflected 30- and 40-deg cases, each having an optimum and a narrow gap. The selection of test cases was based on the flap optimization studies of Wentz,[10] conducted at the WSU in collaboration with NASA. Figure 2 shows the geometry of the flap setting and parameters. It includes the percent-chord X_f and Z_f locations of the optimum gap for 30- and 40-deg flap deflections. When the flap is nested with the main wing, its quarter-chord aerodynamic center at the 0.8125c

Table 1 Test matrix

Cases	δ, deg	G/c	O/c	β, deg
A	0	0	0	0
B	30	0.03	0	21
C	30	0.02	0	33
D	40	0.015	−0.01	67
E	40	0.0115	−0.007	55

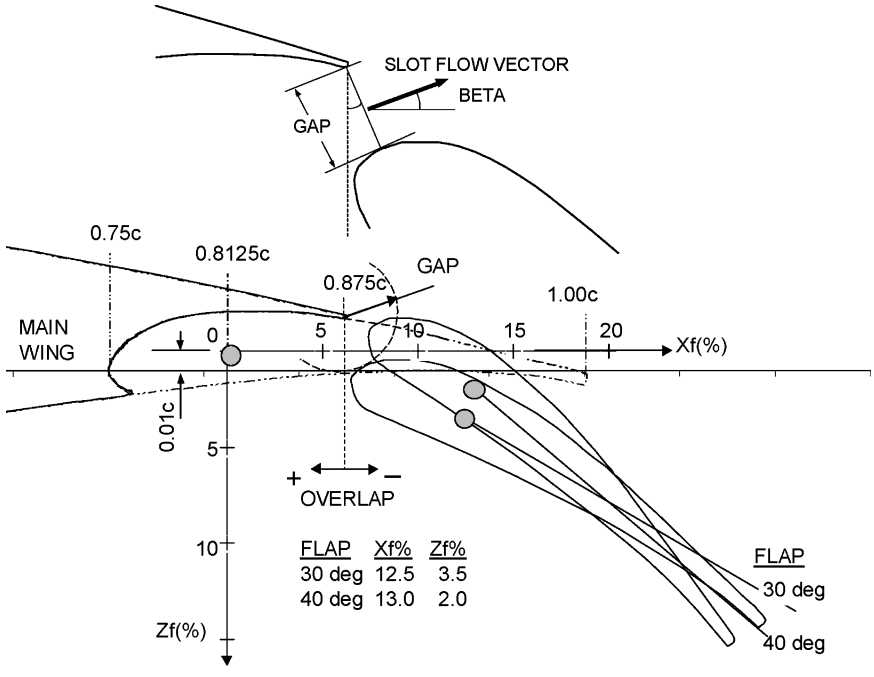

Fig. 2 Geometric view of flap setting parameters for 30- and 40-deg flap deflections.

horizontal and $0.01c$ vertical locations is considered the origin of the X_f and Z_f coordinate system. The flap is rotated in this coordinate system for each flap angle and then translated first in the horizontal and then in the vertical direction to obtain various gaps.

Flap overlap is referenced to a line normal to the main wing trailing edge. It is positive for the flap nose upstream of the reference line and negative for the flap downstream of the line. Flap gap is measured as a minimum radius line for a circle centered at the wing trailing edge ($0.875c$) and tangent to the flap nose. If slot flow is represented in a velocity vector in its centerline, this vector is considered normal to the minimum radius line. The angle that this vector makes with the main wing chord line is a new flap parameter, slot flow angle β. It is, in fact, physically more significant compared to other parameters, as discussed in subsequent sections.

E. Flap Optimization and Effectiveness

To visualize the flap nose position for optimum gaps, flap optimization reported in Ref. 10 is presented here for 30- and 40-deg flap deflections. Figure 3 shows the results for the 30-deg flap case. This is considered to be a typical landing flap configuration. The $C_{l\max}$ contours represent various locations of flap nose for given flap angle. The loci of these contours produce the highest $C_{l\max} = 3.28$, which corresponds to the optimum $G/c = 0.03$ and $O/c = 0.0$. The optimization is also conducted for 40-deg flap, which produced a relatively higher $C_{l\max} = 3.35$, with smaller $G/c = 0.015$ and negative $O/c = -0.01$ as shown in Fig. 4.

The flap effectiveness for the GA(W)-2 airfoil was determined for the optimum gap settings of 30- and 40-deg flap deflections. The additional data for 10- and 20-deg flap deflections are taken from Ref. 10. Figure 5 shows the variation of incremental C_l with flap angle at zero α and $C_{l\max}$ conditions. The $C_{l\max}$ increases with a rate

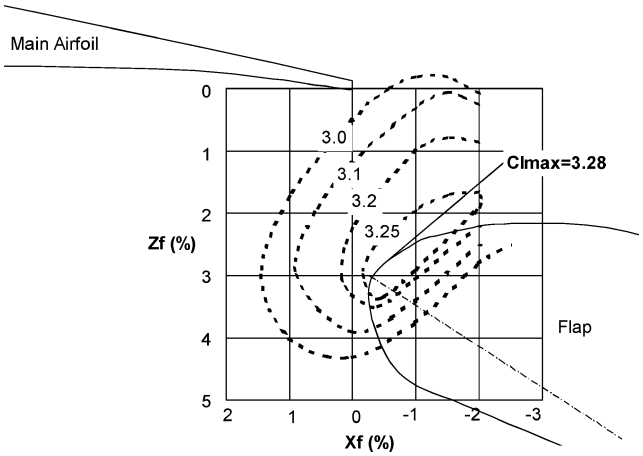

Fig. 3 Flap optimization for 30-deg flap with opt gap (case B), from Ref. 10.

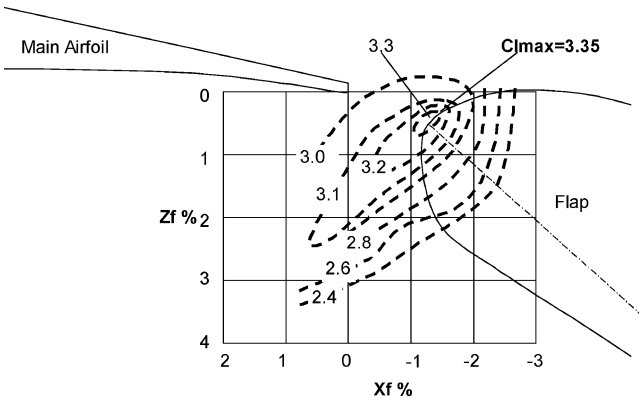

Fig. 4 Flap optimization for 40-deg flap with opt gap (case D), from Ref. 10.

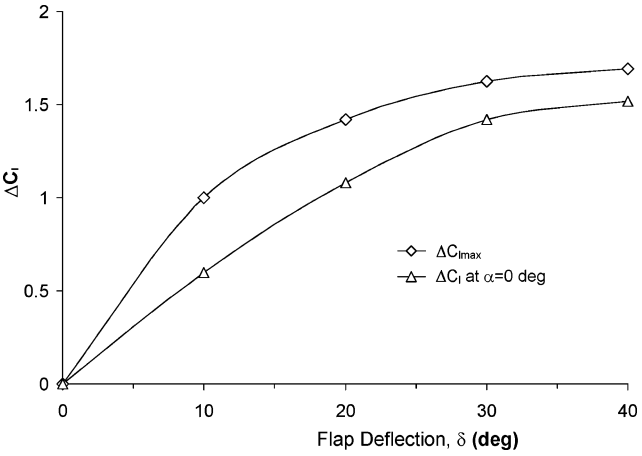

Fig. 5 Flap effectiveness for the airfoil at $\alpha = 0$ deg and $C_{l\max}$ condition.

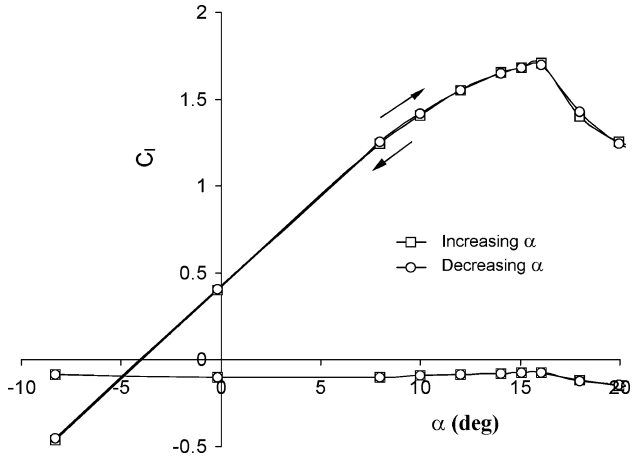

Fig. 6 Absence of hysteresis in C_l and C_m data for flap-nested case A.

of 0.1/deg of the 10-deg flap initially, and then it shows a smaller rate of increase at higher flap deflections and becomes almost zero at the 40-deg flap. The lift coefficient increases at $\alpha = 0$ deg with trends similar to those in $C_{l\max}$ with a lower rate of increase per degree of flap. The flapped airfoil produces its highest incremental $C_{l\max}$ of 1.7 for the 40-deg deflection and a C_l of 1.5 at $\alpha = 0$ deg.

III. Results and Discussion

Experiments were made for the test cases described in Table 1. However, in this section, the results are presented for test cases B, C, and D to have a comparison of flap deflection as well as gap. Lift and moment data are also given for flap-nested case A. Suction peak and trailing-edge C_P values are used to define a pressure recovery factor on both the main wing and the flap. The recovery factor is, in turn, used to evaluate flow separation on airfoil elements. Hot-film velocity data are provided only for case B to show slot flow vectors at near-stall conditions. Slot flow angle is introduced as a new flap design parameter.

A. Hysteresis Effects on Lift and Moment

Figure 6 shows C_l and C_m data for a flap-nested airfoil (case A) at both increasing and decreasing sweep of angle of attack. The airfoil has $C_{l\max} = 1.7$ and $C_m = -0.0759$ at $\alpha = 16$ deg, and $C_l = 0.4$ and $C_m = -0.1$ at $\alpha = 0$ deg. Fixed transition allowed 95%c of the airfoil upper surface to have turbulent boundary-layer flow. The turbulent flow apparently did not have any bubble-induced stall hysteresis.

Figure 7 shows C_l and C_m data for case B at increasing and decreasing α sweep. The airfoil looses 20% of its $C_{l\max} = 3.21$ with an abrupt stall after $\alpha = 13.58$ deg. A value of $C_l = 2.57$ appears, staying almost constant from $\alpha = 14.05$ to 15.55 deg, before another

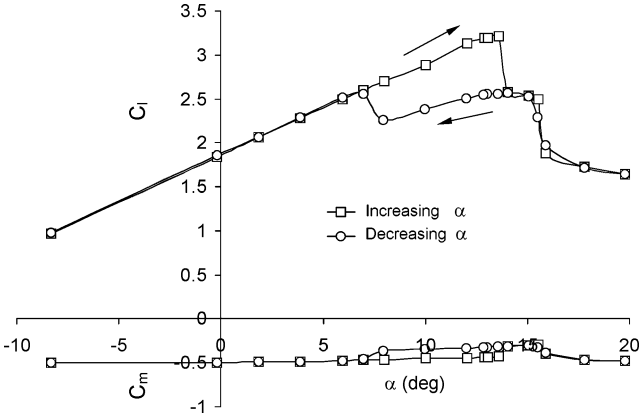

Fig. 7 Stall hysteresis in C_l and C_m data for 30-deg flap with opt gap (case B).

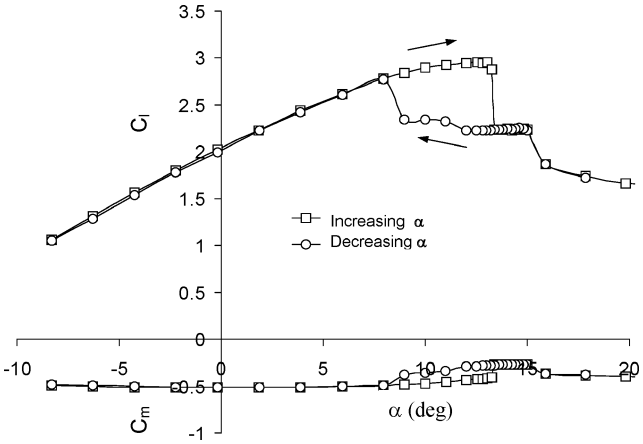

Fig. 8 Stall hysteresis in C_l and C_m data for 30-deg flap with narrow gap (case C).

stall. This peculiar behavior in C_l data was repeatable and better understood when α was lowered back after a few degrees above the second stall. When α passes below 14 deg, the lift coefficient is not restored to its original value (Fig. 7), but instead exhibits a significant loss continuing until $\alpha = 6.95$ deg. The lift curve appears to be shifted downward between $\alpha = 6.95$ and 14.05 deg, indicating the effect of hysteresis. The C_m data, in contrast, shift upward (becomes less negative) in the decreasing side of hysteresis loop.

Narrowing the gap for the 30-deg flap (case C) reduced the α range of hysteresis, as is evident from C_l and C_m data in Fig. 8. The airfoil looses 24.5% of its $C_{l\max} = 2.95$ with an abrupt stall after $\alpha = 13.04$ deg. The poststall $C_l = 2.24$ at $\alpha = 13.61$ remains almost the same until $\alpha = 15.02$ before another stall. The lift coefficient is not restored to its original value when α decreases below 13.61 deg, at least not until $\alpha = 7.96$ deg.

Increasing the flap angle to 40 deg (case D) increased the α range of hysteresis significantly, as shown in Fig. 9. The airfoil looses 38% of its $C_{l\max} = 3.905$ with an abrupt stall after $\alpha = 13.08$ deg. The poststall $C_l = 2.42$ at $\alpha = 13.61$ deg remains almost the same until $\alpha = 15.05$ deg before another stall. The lift coefficient is not restored to its original value when α decreases below 13.54 deg until $\alpha = 0$ deg. For the 40-deg flap case, the C_m data restore their original value at $\alpha = 8$ deg, surprisingly earlier than the corresponding C_l value—possibly due to the reduction in aft airfoil loading.

B. Hysteresis Effects on C_P Distribution

With knowledge of the range of the hysteresis loop from force and moment data, surface pressure distributions were obtained to study the flowfield on airfoil elements for flap cases B, C, and D. The measurements were made at α settings determined by α limits and the $C_{l\max}$ condition of hysteresis loop in lift curves.

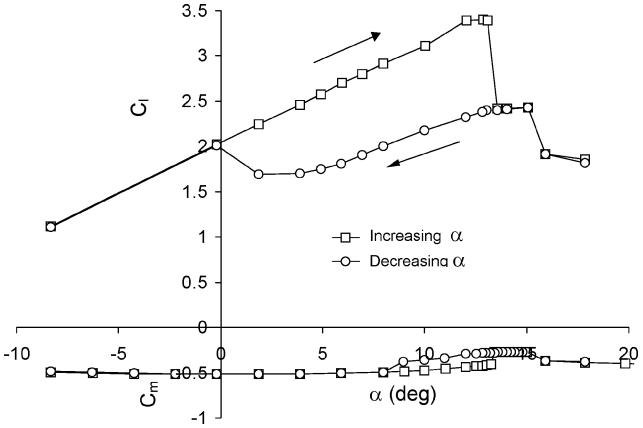

Fig. 9 Stall hysteresis in C_l and C_m data for 40-deg flap with opt gap (case D).

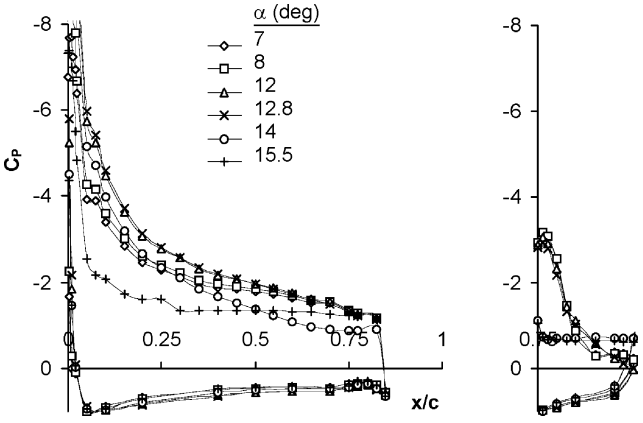

Fig. 10 C_p distribution at $\alpha = 7, 8, 12, 12.8, 14$, and 15.5 deg for 30-deg flap with opt gap (case B) with increasing α.

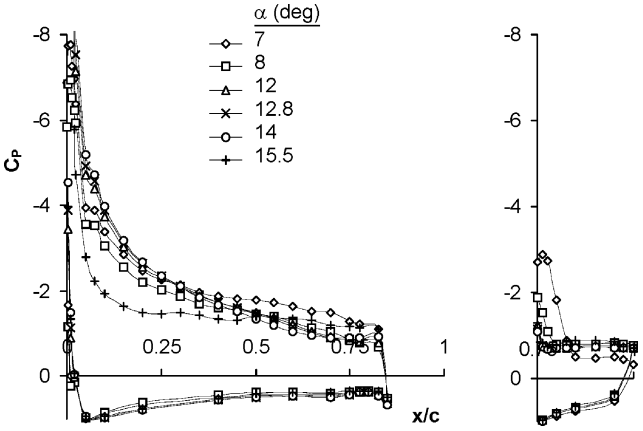

Fig. 11 C_p distribution at $\alpha = 7, 8, 12, 12.8, 14$, and 15.5 deg for 30-deg flap with opt gap (case B) with decreasing α.

For the 30-deg flap with optimum gap (case B), the C_p distribution was obtained at $\alpha = 7$, 8, 12, 12.8, 14, and 15.5 deg. The data for an increasing α side are shown in Fig. 10 and for a decreasing α side in Fig. 11. By the comparison of Figs. 10 and 11, there is almost no discrepancy seen between the increasing and decreasing α sides at α limits (7 and 14 deg) of the hysteresis loop. The highest discrepancy occurs at $\alpha = 12.8$ deg, which is near the $C_{l\max}$ angle, as shown in Fig. 12. The suction C_P values on the main wing are lower for the decreasing side because the flap apparently does not provide the necessary downwash, and consequently the circulation for the main wing, in contrast to the case for the increasing angle of attack. For both sides of the loop, suction C_P on the main wing

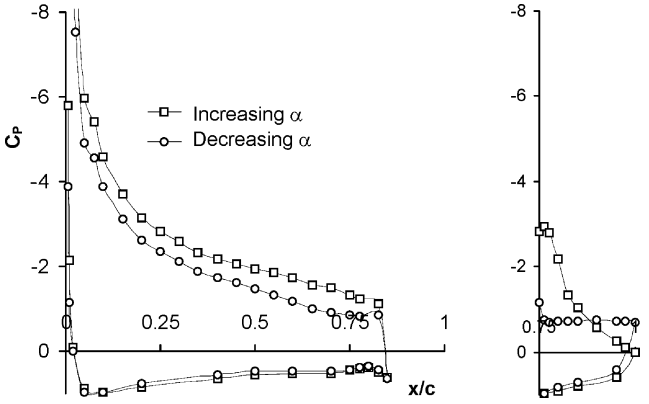

Fig. 12 Hysteresis effect in C_p distribution at $\alpha = 12.8$ deg for 30-deg flap with opt gap (case B) with increasing and decreasing α.

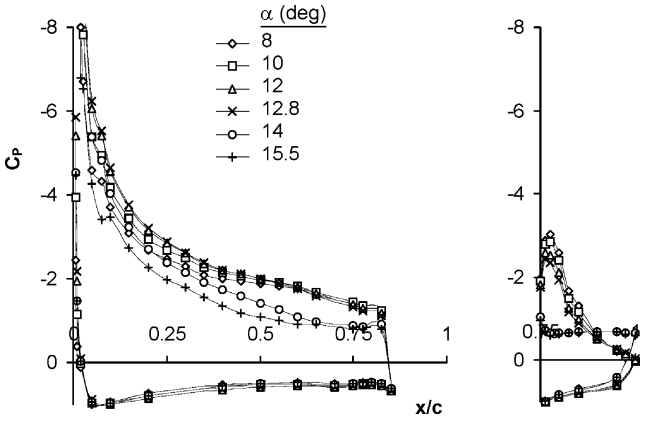

Fig. 13 C_p distribution at $\alpha = 8, 10, 12, 12.8, 14$, and 15.5 deg for 30-deg flap with narrow gap (case C) with increasing α.

shows a dramatic fall after its peak value near the leading edge. The dramatic fall is followed by a short step between the 5 and 7.5% chord locations, where the transition is fixed on the upper surface. The trip strips apparently produced a short bubble to trip the flow. This was also evident from surface flow visualizations. At a low α setting, the aft portion of flap has a nearly constant C_P distribution, as shown in Fig. 10. The start of constant C_P is considered to be the location for flow separation, as evidenced in correlation to the flow visualization studies. The region of separated flow on flap decreases with increasing α settings and almost disappears at $\alpha = 12.8$ deg before the stall. This is considered to be a typical feature of flaps designed to maximize the $C_{l\max}$ of the airfoil system.[10] At poststall $\alpha = 14$ deg, suction C_P values on the flap are flattened, indicating a leading-edge stall. The flatness on the flap moves upstream onto the main wing, and, at a higher $\alpha = 15.5$ deg, it leads to a massive flow separation. When α is lowered back from 14 deg, the flow on the flap remains stalled until $\alpha = 7$ deg, where the airfoil lift is restored to its value obtained with increasing α. In other words, the suppressed C_P values on the flap under the influence of the thickening wing wake after the first stall are evidently not returned to their prestall values until a significant reduction in α occurs.

For the 30-deg flap with a narrow gap (case C), the C_p distribution was obtained at $\alpha = 8$, 10, 12, 12.8, 14, and 15.5 deg. The data for the increasing α side are shown in Fig. 13 and for the decreasing α side in Fig. 14. Unlike the optimum case B, the suction C_P values on the flap do not show a separated region at prestall $\alpha = 8$ deg, and they stay almost the same until $\alpha = 12.8$ deg. This corresponds to the lift curve rounding near the $C_{l\max}$ condition (Fig. 8). The data show almost no discrepancy at $\alpha = 8$ deg, whereas they show some discrepancy at $\alpha = 14$ deg. The highest discrepancy between the increasing and decreasing α sides occurs at $\alpha = 12.8$ deg, as shown in Fig. 15. As α increases to 15.5 deg, the flow separation moves upstream on the main wing, but not enough to cause a leading-edge stall.

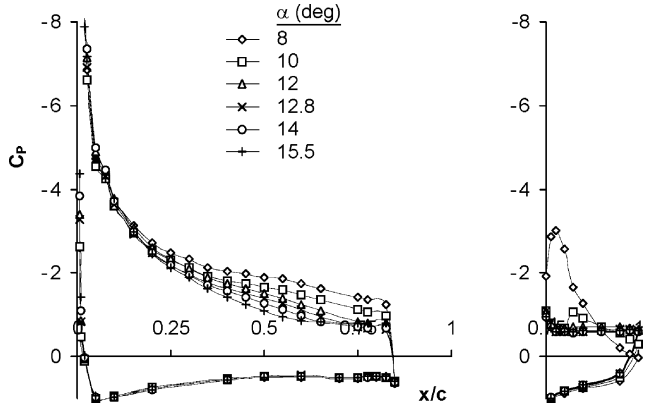

Fig. 14 C_P distribution at $\alpha = 8, 10, 12, 12.8, 14$, and 15.5 deg for 30-deg flap with narrow gap (case C) with decreasing α.

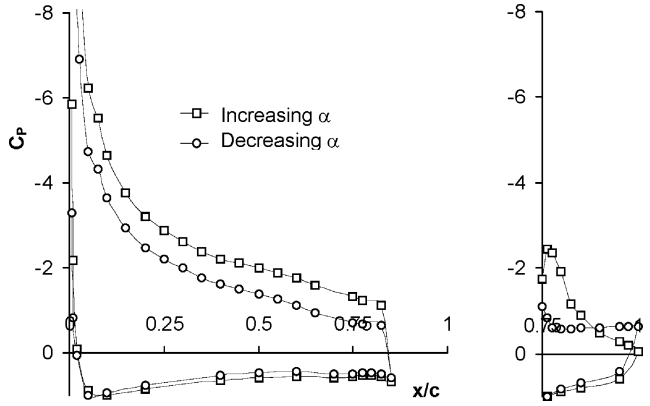

Fig. 15 Hysteresis effect in C_p distribution at $\alpha = 12.8$ deg for 30-deg flap with narrow gap (case C) with increasing and decreasing α.

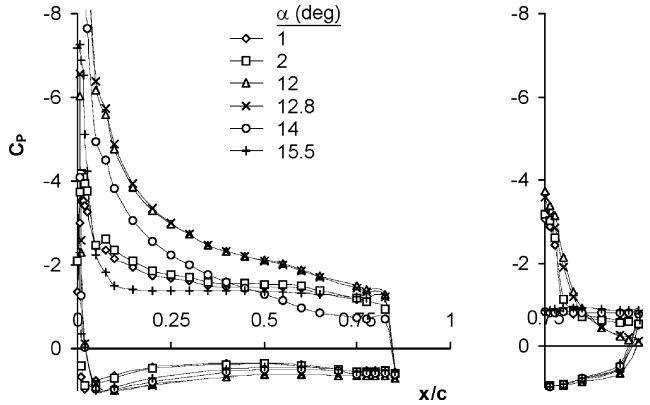

Fig. 16 C_p distribution at $\alpha = 1, 2, 12, 12.8, 14$, and 15.5 deg for 40-deg flap with opt gap (case D) with increasing α.

For the 40-deg flap with optimum gap (case D), the C_p distribution was obtained at 1, 2, 12, 12.8, 14, and 15.5 deg. The data for the increasing α side are shown in Fig. 16 and for the decreasing α side in Fig. 17. The C_P data show the highest discrepancy between the increasing and decreasing α sides at $\alpha = 12.8$ deg (Fig. 18) and almost no discrepancy at the α limits (2 and 14 deg) of the loop. Note that the corresponding lift curve in Fig. 9 shows the lower end of the hysteresis loop at $\alpha = 0$ deg. The start of hysteresis for this case would be better shown by selecting another α setting, for example, 3 deg. The flow separation on the flap disappears as the α setting increases from 2 to 12 deg, leading to the highest $C_{l\max}$ condition.

C_P distributions at each α setting were integrated to find individual lift contributions from the wing and flap components. The integration was made by the trapezoidal method in chord line intervals

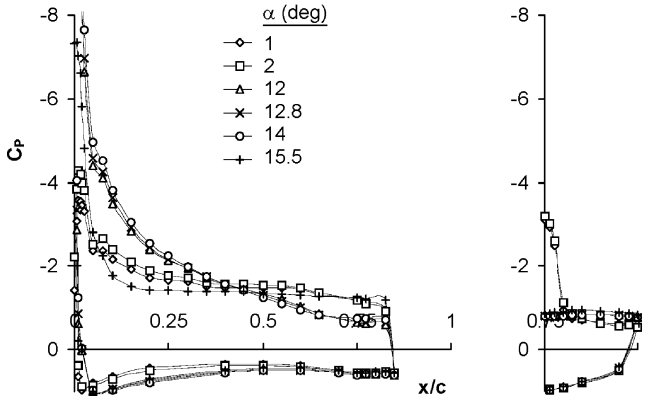

Fig. 17 C_p distribution at $\alpha = 1, 2, 12, 12.8, 14$, and 15.5 deg for 40-deg flap with opt gap (case D) with decreasing α.

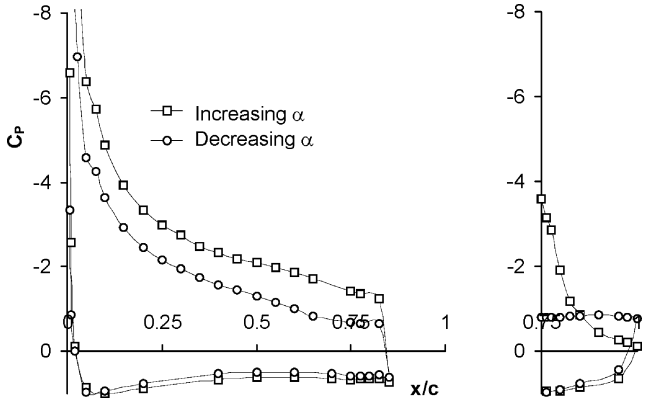

Fig. 18 Hysteresis effect in C_p distribution at $\alpha = 12.8$ deg for 40-deg flap with opt gap (case D) with increasing and decreasing α.

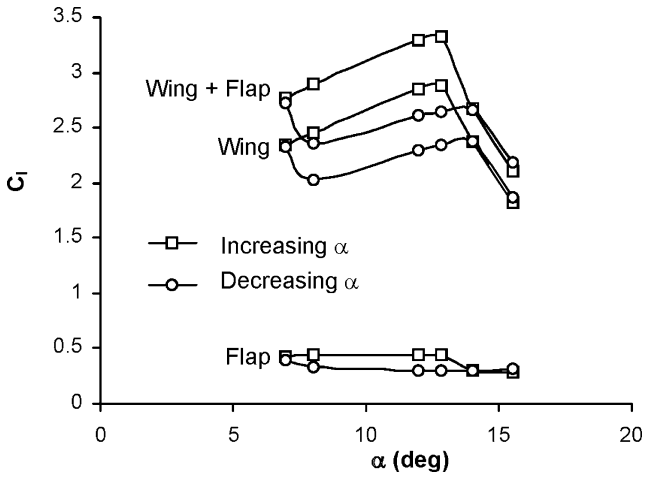

Fig. 19 C_l values from integrated C_P distributions on wing alone, flap alone, and wing plus flap for case B with increasing and decreasing α.

given with airfoil coordinates. With all test cases considered, the integrated C_l was very close to or at most 4% higher than the corresponding balance C_l. Figures 19–21 show C_l variation with α settings for all three flap cases studied. For all cases, flap C_l stays almost constant for both increasing and decreasing α sides of the hysteresis loop. Its addition shifts the wing C_l upward to build up total airfoil C_l. When $\alpha = 12.8$ deg, flap C_l is only 13.1, 11.8, and 12.5% of total airfoil C_l for cases B, C, and D, respectively. The data show that the flap C_l is not very sensitive to changes in α until the stall, but the main wing is, and it is similar to that on single airfoils. Flap apparently has the effect of boosting the circulation of the main wing, which has the majority of total airfoil C_l. The circulation on

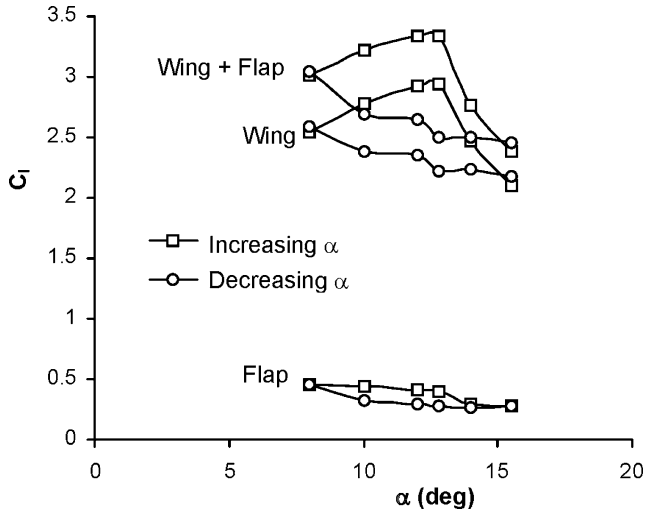

Fig. 20 C_l values from integrated C_P distributions on wing alone, flap alone, and wing plus flap for case C with increasing and decreasing α.

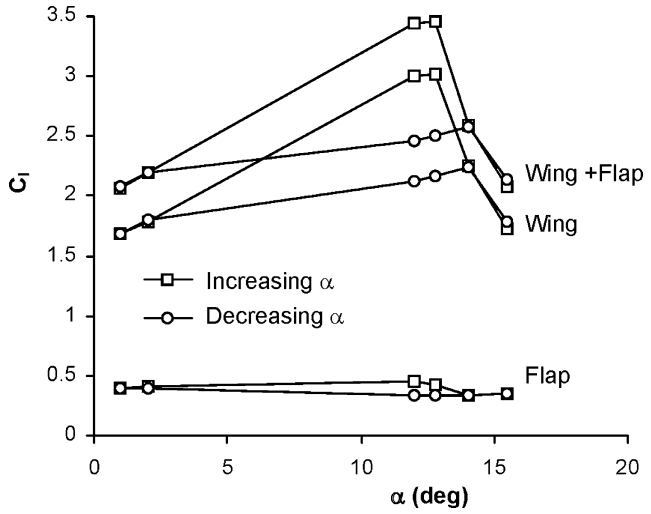

Fig. 21 C_l values from integrated C_P distributions on wing alone, flap alone, and wing plus flap for case D with increasing and decreasing α.

the main wing, in turn, effectively reduces the flap α, as well as the velocities on its surface and, hence, reduces its lift.[7]

C. Recovery Factor on C_P Distributions

C_P distributions on the upper surface of the airfoil elements exhibited a suction peak followed by a region of recovery to a pressure value near the trailing edge. The region of pressure recovery is of critical importance because of its strong influence on flow separation. For practical uses, it is defined in Ref. 11 by a coefficient factor, as follows:

$$C_{\mathrm{PR}} = \frac{C_{P@0.95c} - C_{P\,\min}}{1 - C_{P\,\min}}$$

The pressure recovery coefficient C_{PR} is, in fact, derived from the canonical pressure coefficient described by Smith.[7] Here, $C_{P\,\min}$ and $C_{P@0.95c}$ are the pressure coefficient values at the point of minimum pressure and the point of maximum pressure recovery, respectively. The point of maximum pressure recovery was assumed to be at the 95%c location of airfoil elements, corresponding to port locations at 0.775c for the wing and 0.975c for the flap. These pressure coefficient values were determined from C_P distributions and plotted against α to show their effects on the main wing and flap.

Peak suction pressure coefficient $C_{P\,\min}$ on both the wing and flap is shown in Fig. 22 for an optimum gap case of 30-deg flap. It corresponds to the location for the maximum velocity or start of

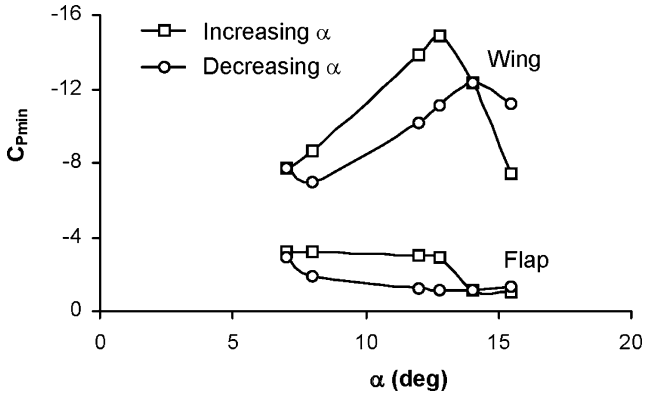

Fig. 22 Peak suction C_P values on wing and flap for case B with increasing and decreasing α.

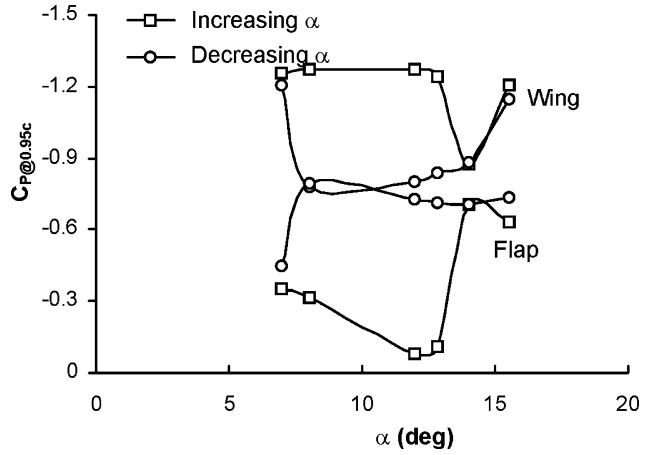

Fig. 23 C_P values at 0.95c of wing and flap upper surface for case B with increasing and decreasing α.

pressure rise on each airfoil element. Wing $C_{P\,\min}$ has a maximum of -14.9 at $\alpha = 12.8$ deg, followed by a 25% drop with stall. It does not reach its original $C_{P\,\min}$ value for the decreasing α side until α is lowered from 14 deg all of the way down to 7 deg, as in the corresponding lift curve. The flap $C_{P\,\min}$ is apparently suppressed by the boundary-layer wake from the main wing and shows no sensitivity to changes in α until the stall. It has a value of -2.95 at $\alpha = 12.8$ deg, followed by a drop to -1.12 at $\alpha = 14$ deg, and stays about this low for the decreasing α side of the loop. The flap $C_{P\,\min}$ is, in fact, located slightly downstream of main wing trailing edge, where the wake flow having the suction $C_{P@0.95c}$ is discharged into the slot flow region.

The pressure coefficient at the 95%c upper surface $C_{P@0.95c}$ on both the wing and the flap is shown in Fig. 23 for case B. Wing $C_{P@0.95c}$ values are not sensitive to changes in α until the stall. It is -1.239 at $\alpha = 12.8$ deg, followed by a drop to -0.873 at $\alpha = 14$ deg. Flap $C_{P@0.95c}$ value, in contrast, decreases slightly (becomes less negative) with increasing α and becomes -0.111 at $\alpha = 12.8$ deg, followed by a jump to -0.706 at $\alpha = 14$ deg. The wing and flap values apparently approach each other with the stall. They become closer for the decreasing α side and have a common value of -0.783 at $\alpha = 8$ deg before each returns to its original value.

Pressure recovery factor C_{PR} correlates the $C_{P\,\min}$ to the $C_{P@0.95c}$ through its definition shown earlier. Its variation on both the wing and the flap is shown in Fig. 24 for case B. Wing C_{PR} increases from 0.75 at $\alpha = 7$ to a maximum of 0.86 at $\alpha = 14$ deg and shows no significant difference from the decreasing α side. Flap C_{PR}, in contrast, goes from 0.67 at $\alpha = 7$ to 0.71 at $\alpha = 12.8$ and then drops sharply to 0.18 at $\alpha = 14$ deg. Its maximum occurs simultaneously with the flapped airfoil $C_{l\,\max}$. When α is lowered from 14 deg, the flap C_{PR} values show a large discrepancy from those of the increasing α side. This type of behavior in wing and flap C_{PR} values was also

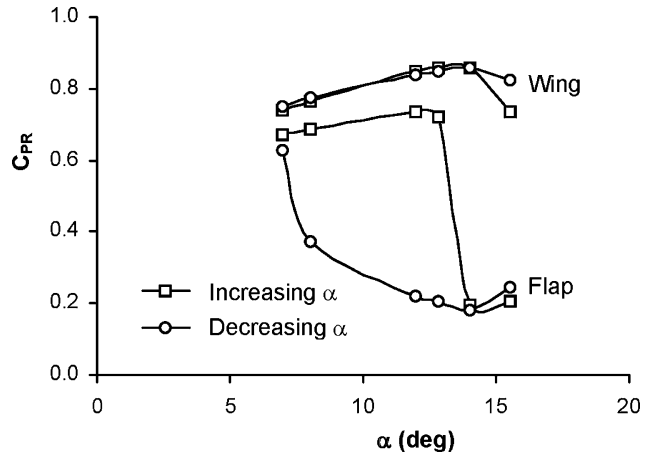

Fig. 24 Pressure recovery factors on wing and flap for case B with increasing and decreasing α.

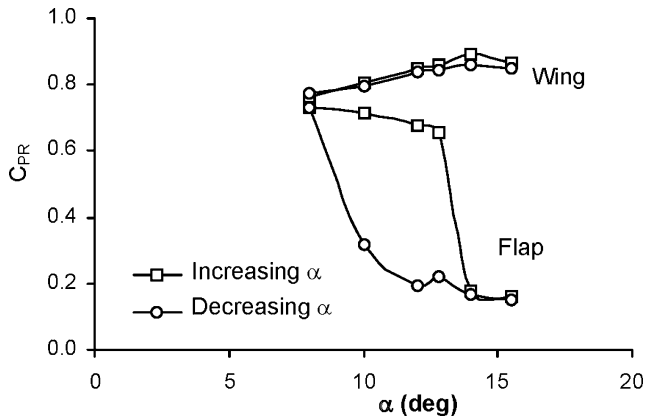

Fig. 25 Pressure recovery factors on wing and flap for case C with increasing and decreasing α.

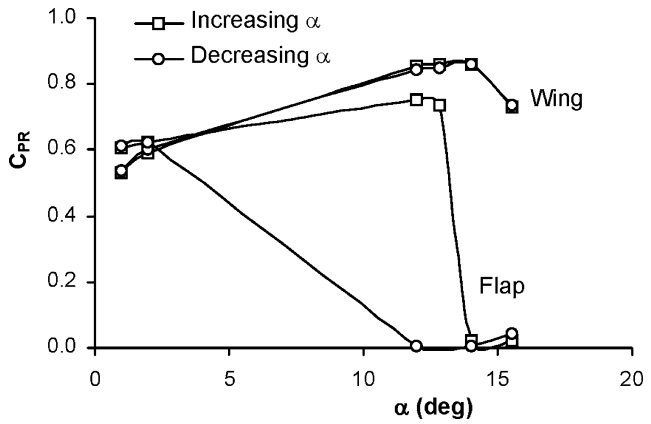

Fig. 26 Pressure recovery factors on wing and flap for case D with increasing and decreasing α.

observed for recovery factor for the narrow gap case C and higher flap angle case D, as shown in Figs. 25 and 26, respectively. These flap gap cases B–D are compared in Fig. 27 for the increasing α side only. Wing C_{PR} values are nearly independent of flap setting and appear to depend primarily on α, even though lift coefficient and minimum C_P values are strongly influenced by the flap deflection. Flap C_{PR} values, however, show variations with α before the stall. Case D has the highest values, but maintains the same slope as case B. Case C shows a decreasing trend in slope until the stall.

The recovery factor C_{PR}, in general, has a critical value for which separation first develops. The critical value (shown in Fig. 27) is about 0.72 on the flap, experiencing the abrupt stall at $\alpha = 12.8$ deg,

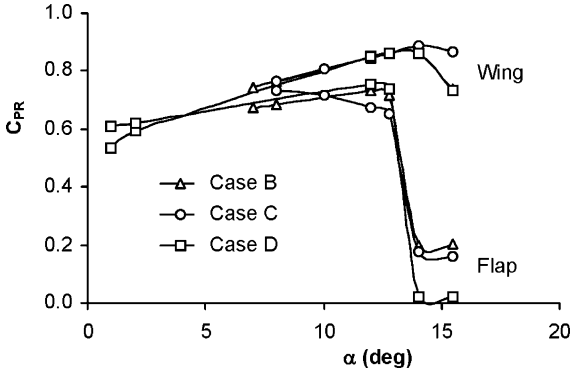

Fig. 27 Comparison of pressure recovery factor for cases B, C, and D on wing and flap, increasing α sweep only.

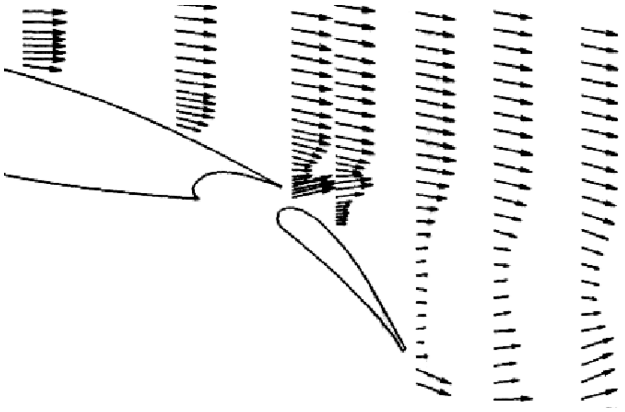

Fig. 28 Hot-film velocity vectors on flap flowfield for case B.

earlier than the main wing, which has its peak 0.86 at $\alpha = 14$ deg. The critical C_{PR} corresponds to a maximum pressure recovery at a 95%c location. This C_{PR} can, in fact, be used as a design parameter as suggested in Ref. 11. For an inverse airfoil design, C_P distribution is typically modified according to design specifications. With the modification, the $C_{P\,\min}$ and $C_{P@0.95c}$ values could be set to produce the desired C_{PR} value. In this way, airfoil contour is also changed. The changes in airfoil contour may result in a favorable effect on separation and stall, but not enough to alleviate the hysteresis problem in a flapped airfoil. There is also the effect of slot flow, which appears significant, as discussed in the subsequent section.

D. Slot Flow Orientation

Slot flow orientation was studied using oil dot flow visualization and hot-film probe measurements.[8,9] Figure 28 shows the hot-film velocity vectors of flap region for case B at $\alpha = 12.8$ deg. The hot-film data were obtained for a given α after settling of the test flow produced by increasing airspeed in the tunnel. Boundary-layer and wake deficits are clearly visible on the velocity profiles. The vector data represent the results of horizontal and vertical velocity components. They are relatively high at the flap trailing edge and inclined downward; however, they are inclined upward for the region of slot flow as depicted at the first survey station above the flap leading edge. The hot-film data were taken as much as 6.35 mm away from the surface for probe safety. The slot flow was also visualized by oil dots located at one-side 25.4 mm square grid points of a splitter plate about one chord long (which is not to be confused with the splitter plate pressure probe also used in the experimental program[8]). The plate was large enough to cover the separated flowfield and wake of airfoil elements. Oil flow patterns and velocity vectors were in agreement and showed the upward inclination of slot flow with respect to the freestream flow. This type of flow inclination in velocities, perhaps at a smaller degree, can also be seen in other published data.[12–14]

The flowfield data clearly show that the slot flow does not tend to follow the flap nose curvature closely because of an upward inclination. The inclination was higher for the 40-deg flap case with its nose position shown in Fig. 4. The slot flow angle β is, in fact, a measure of this inclination as shown in Fig. 2 and is sensitive to changes in overlap and contour of the flap nose. The slot flow angle was computed for various flap pivot locations, producing the same gap as the optimum for each flap deflection. The calculated β values seem to correlate geometrically with the orientation of slot flow determined by hot-film velocities above the flap nose.

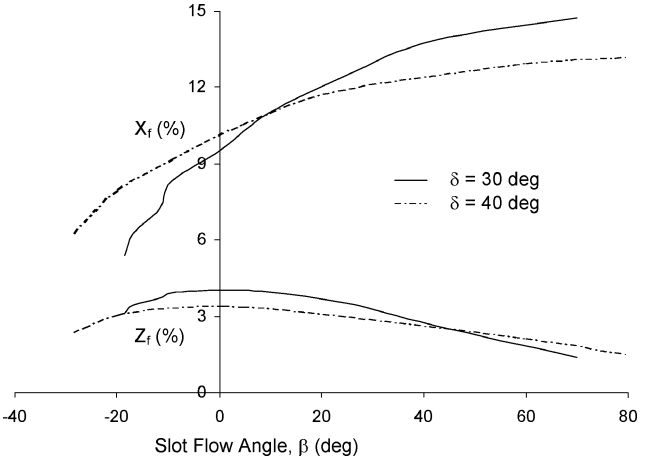

Fig. 29 Variation of flap pivot locations with slot flow angle β for 30- and 40-deg flap with opt gaps (cases B and D, respectively).

Figure 29 shows β variation with X_f and Z_f percent flap pivot locations for 30- and 40-deg deflections. The optimum flap settings shown in Fig. 2 have positive β values for both flap deflections. The angle β is 24 deg for the $\delta = 30$ deg and 64 deg for the $\delta = 40$ deg flap cases. These values are slightly different from those provided in Table 1 (also given in Ref. 4) due to some smoothing involved with the flap surface. When $\beta = 0$ deg, $X_f = 9.5$ and 10.2% and $Z_f = 4.0$ and 3.4% for the $\delta = 30$ and 40-deg flaps, respectively. Both zero and negative β values would result in some flap overlap, for which the slot flow would be directed over the flap. The inclined slot flow would, in fact, promote favorable pressure gradients on the flap upper surface and, hence, delay possible flow separation. However, increasing overlap, the flap nose gets closer to the cove separation bubble, and this may reduce the effective gap size due to the presence of boundary layers. This requires gap optimization conducted as close to the flight Reynolds number as possible. Also, the overlapped section of the flap nose does not produce suction pressure, but provides a passage for the slot flow.

The best location for the landing flap has traditionally been obtained by finding a location for the flap nose that results in the highest maximum lift coefficient. It is suggested here that the flap be optimized with consideration of hysteresis effects by using the additional flap parameter β to determine the slot flow orientation. For each flap angle and gap setting, there seems to be an optimum β value that results in significant reduction, if not elimination, of hysteresis effects. The optimum β value can be determined with further research and, hence, requires wind-tunnel tests of this kind.

IV. Conclusions

Stall hysteresis discovered in the wind-tunnel performance of a flapped GA(W)-2 airfoil is further examined by using the data obtained for C_P distribution and the hot-film velocity vector, in addition to force and moment characteristics reported earlier. Based on the results of experiments, the following conclusions can be drawn:

1) Flow separation present on the flap at low α disappears at the $C_{l\,\max}$ condition. Flap C_P distribution under the influence of main wing wake is not sensitive to changes in α until stall. With the first stall, flap suction pressures are suppressed by the thickening of the main wing wake. The suppressed pressures are apparently not reversible to their prestall values until the angle of attack is lowered significantly.

2) Pressure recovery on airfoil elements can be described by a coefficient factor. The peak value for the recovery factor occurs on the flap simultaneously with the flapped airfoil $C_{l\max}$. The limiting separation value for the recovery factor, considered as a design parameter, can be used to modify C_P distribution for desired flap contour.

3) Slot flow velocities with an upward inclination indicate a reduction of circulation effect over the main wing. The slot flow orientation described by a new flap parameter β, is more sensitive to changes in flap position and contour.

4) It is suggested that the flap design include the use of a slot flow angle to describe the slot flow orientation and a limiting pressure recovery factor to select a proper contour for the flap upper surface.

References

[1]Mueller, T. J., "Low Reynolds Number Vehicles," AGARDograph 288, Feb. 1985.

[2]Marchman, J. F., "Aerodynamic Testing at Low Reynolds Numbers," *Journal of Aircraft*, Vol. 24, No. 2, 1987, pp. 107–114.

[3]Biber, K., "An Overview of Steady and Dynamic Airfoil Performance," Society of Automotive Engineers, SAE Paper 93-1228, May 1993.

[4]Biber, K., and Zumwalt, G. W., "Hysteresis Effects on Wind Tunnel Measurements of a Two-Element Airfoil," *AIAA Journal*, Vol. 31, No. 2, 1993, pp. 326–330.

[5]Landman, D., and Britcher, C. P., "Experimental Investigation of Multielement Airfoil Lift Hysteresis due to Flap Rigging," *Journal of Aircraft*, Vol. 38, No. 4, 2001, pp. 703–708.

[6]Foster, D. N., Irwin, H. P. A., and Williams, B. R., "The Two-Dimensional Flow Around A Single Slotted Flap," Royal Aircraft Establishment, R&M 3671, Farnborough, England, U.K., Sept. 1971.

[7]Smith, A. M. O., "High-Lift Aerodynamics," *Journal of Aircraft*, Vol. 12, No. 6, 1975, pp. 501–530.

[8]Biber, K., and Zumwalt, G. W., "An Experimental Study of a Two-Element Airfoil with Large Separation," AIAA Paper 92-0267, Jan. 1992.

[9]Biber, K., and Zumwalt, G. W., "Flowfield Measurements on a Two-Element Airfoil with Large Separation," *AIAA Journal*, Vol. 31, No. 3, 1993, pp. 459–464.

[10]Wentz, W. H., Jr., "Wind Tunnel Tests of the GA(W)-2 Airfoil with 20% Aileron, 25% Slotted Flap, 30% Fowler Flap and 10% Slot-Lip Spoiler," NASA CR-145139, 1977.

[11]Wentz, W. H., Jr., "Use of Simplified Flow Separation Criteria for Slotted Flap Design," Society of Automotive Engineers, SAE 77-0481, March–April 1977.

[12]Braden, J. A., Whipkey, R. R., Jones, G. S., and Lilley, D. E., "Experimental Study of the Separating Confluent Boundary Layer," Vol. 1, Summary, NASA CR 3655, March 1983.

[13]Braden, J. A., Whipkey, R. R., Jones, G. S., and Lilley, D. E., "Experimental Study of the Separating Confluent Boundary Layer," Vol. 2, Experimental Data, NASA CR 166018, March 1983.

[14]Wentz, W. H., Jr., and Ostawari, C., "Additional Flow Field Studies of the GA(W)-1 Airfoil with 30-Percent Chord Fowler Flap Including Slot-Gap Variations," NASA CR 3687, May 1983.